

# SOLITON, BREATHER AND ROGUE WAVE SOLUTIONS FOR SOLVING THE NONLINEAR SCHRÖDINGER EQUATION USING A DEEP LEARNING METHOD WITH PHYSICAL CONSTRAINTS

JUNCAI PU, JUN LI, AND YONG CHEN

**ABSTRACT.** The nonlinear Schrödinger equation is a classical integrable equation which contains plenty of significant properties and occurs in many physical areas. However, due to the difficulty of solving this equation, in particular in high dimensions, lots of methods are proposed to effectively obtain different kinds of solutions, such as neural networks, among others. Recently, a method where some underlying physical laws are embedded into a conventional neural network is proposed to uncover the equation's dynamical behaviors from spatiotemporal data directly. Compared with traditional neural networks, this method can obtain remarkably accurate solution with extraordinarily less data. Meanwhile, this method also provides a better physical explanation and generalization. In this paper, based on the above method, we present an improved deep learning method to recover the soliton solutions, breather solution and rogue wave solutions to the nonlinear Schrödinger equation. In particular, the dynamical behaviors and error analysis about the one-order and two-order rogue waves of the Schrödinger equation are revealed by the deep neural network for the first time. Moreover, the effects of different numbers of initial points sampled, residual collocation points sampled, network layers, neurons per hidden layer on the one-order rogue wave dynamics of this equation have been considered with the help of the control variable way under the same initial and boundary conditions. Numerical experiments show that the dynamical behaviors of soliton solutions, breather solution and rogue wave solutions of the integrable nonlinear Schrödinger equation can be well reconstructed by utilizing this physically-constrained deep learning method.

## 1. INTRODUCTION

In recent decades, more and more attention have been paid to the nonlinear problems in fluid mechanics, condensed matter physics, optical fiber communication, plasma physics and even biology [1–4]. After establishing nonlinear partial differential equations to describe these nonlinear phenomena and then analyzing the analytical and numerical solutions of these nonlinear models, the essence of these nonlinear phenomena can be understood [5]. Therefore, the research of these nonlinear problems is essentially transformed into the study of nonlinear partial differential equations which describe these physical phenomena. Due to many basic properties of linear differential equations are not applicable to nonlinear differential equations, these nonlinear differential equations which the famous nonlinear Schrödinger equation belongs to are more difficult to solve compared with the linear differential equations. It is well known that the Schrödinger equation can be used to describe the quantum behavior of microscopic particles in quantum mechanics [6]. Furthermore, various solutions of this equation can describe the nonlinear phenomena in other physical fields, such as optical fiber, plasma, Bose-Einstein condensates, fluid mechanics and Heisenberg ferromagnet [7–15]. While, the research on the exact solutions of the nonlinear Schrödinger equation has made great progress, the “curse of dimensionality” phenomena often occurs during solving this equation, especially in quantum N-body problems [16].

With the explosive growth of available data and computing resources, deep neural networks, i.e., deep learning [29], are applied in many areas including image recognition, video surveillance, natural language processing, medical diagnostics, bioinformatics, financial data analysis and so on [17–22, 26]. In scientific computing, especially, the neural network method [23–25] provides an ideal representation for the solution of differential equations [28] due to its universal approximation properties [27]. Recently, a physically constrained deep learning method called physics-informed neural network (PINN) [30] and its improvement [31] has been proposed which is particularly suitable for solving differential equations and corresponding inverse problems. It is found that the PINN architecture can obtain remarkably accurate solution with extraordinarily less data. Meanwhile, this method also provides a better physical explanation for predicted solutions because of the underlying physical constraints which is usually described explicitly by the differential equations. In this paper, the computationally efficient physics-informed data-driven algorithm for inferring solutions to more general nonlinear partial differential equations, for example the integrable nonlinear Schrödinger equation, is studied.

As is known to all, the study of exact solutions for integrable equations which are used to describe complex physical phenomena in the real world have been paid more and more attention in plasma physics, optical fiber, fluid dynamics and others fields [13, 32–35]. The Hirota bilinear method, the symmetry reduction method, the Darboux transformation, the Bäcklund transformations, the inverse scattering method and the function expansion method are powerful means to solve nonlinear integrable equations, and many other methods are based on them [5, 36–41]. Although the computational cost of some direct numerical solutions of integrable equations is very high, with the revival of neural networks, the development of more effective deep learning algorithms to obtain data-driven solutions of nonlinear integrable equations has aroused great interest [42–46]. Li et al. [42, 45, 46] constructed abundant numerical solutions of second-order and third-order nonlinear integrable equations with different initial and boundary conditions

by deep learning method based on the PINN model. Previous works mainly focused on some simple solutions (e.g., N-soliton solutions, kink solutions) of given system or integrable equation. As far as we know, the soliton solutions, breather solution and rogue wave solutions [8,9] of the integrable nonlinear Schrödinger equation have not been given out by the deep learning method based on PINN. Therefore, we introduce the deep learning method with underlying physical constraints to construct the soliton solutions, breathing solution and rogue wave solutions of integrable nonlinear Schrödinger equation in this work.

This paper is organized as follows. In section 2, we introduce the physically constrained deep learning method and briefly present some problem setups. In Section 3, the one-soliton solution and two-soliton solution of the nonlinear Schrödinger equation is obtained by this approach, and the breather solution are derived compared with the two-soliton solution. Section 4 provides rogue wave solutions which contain one-order rogue wave and two-order rogue wave for the nonlinear Schrödinger equation, and the relative  $\mathbb{L}_2$  errors of simulating the one-order rogue wave of nonlinear Schrödinger equation with different numbers of initial points sampled, residual collocation points sampled, network layers and neurons per hidden layer are also given out in detail. Conclusion is given in last section.

## 2. METHOD

In this paper, we will consider (1+1)-dimensional nonlinear time-dependent integrable equations, in which each partial differential equation contains dispersion terms as well as other partial derivatives, and the general form of (1+1)-dimensional integrable equations as follows

$$q_t + \mathcal{N}(q, q_x, q_{xx}, q_{xxx}, \dots) = 0, \quad (2.1)$$

where  $q$  are complex-valued solutions of  $\{x, t\}$  to be determined later, and  $\mathcal{N}$  is arbitrary combination of linear term and nonlinear term that containing solution  $q$  and derivative of  $q$  to  $x$ . In addition, in order to ensure that Eq. (2.1) have better integrability and more abundant solutions, equations (2.1) need to satisfy integrable properties such as Painlevé integrability, Lax integrability, Liouville integrability and so on [32, 47, 48]. These theories have been very complete in the direction of integrable systems. Based on the theory of integrable systems and PINN, we establish a deep learning method to approximate the potential complex value solution  $q(x, t)$  of integrable equations. This method enables us to open the black box by understanding and appreciating the key role of automatic differential mechanism in the field of deep learning [49]. Here, we use the exact same automatic differentiation techniques, employed by the deep learning community, to neural networks by taking their derivatives with respect to their input coordinates (i.e., space  $x$  and time  $t$ ) where the constraint is described by integrable equations. We have simply observed that this structured approach introduces a regularization mechanism that allows us to use relatively simple feed-forward neural network architectures and train them with small amounts of data. Considering the complexity of the structure of complex valued solution  $q(x, t)$ , we decompose  $q(x, t)$  into real part  $u(x, t)$  and imaginary part  $v(x, t)$ , i.e.  $q = u + iv$ . Of course, here  $u(x, t)$  and  $v(x, t)$  are real valued functions. Then substituting into Eq. (2.1), we have

$$u_t + \mathcal{N}_u(u, u_x, u_{xx}, u_{xxx}, \dots) = 0, \quad (2.2)$$

$$v_t + \mathcal{N}_v(v, v_x, v_{xx}, v_{xxx}, \dots) = 0. \quad (2.3)$$

We define the network respectively  $f_u(x, t)$ ,  $f_v(x, t)$  to be given by the left-hand-side of Eq. (2.2) and (2.3)

$$f_u := u_t + \mathcal{N}_u(u, u_x, u_{xx}, u_{xxx}, \dots), \quad (2.4)$$

$$f_v := v_t + \mathcal{N}_v(v, v_x, v_{xx}, v_{xxx}, \dots), \quad (2.5)$$

and the solution  $q(x, t)$  is trained to satisfy the physical constraint condition (2.4) and (2.5) which play a vital role of regularization and have been embedded into the mean-squared objective function (Loss function)

$$Loss = Loss_u + Loss_v + Loss_{f_u} + Loss_{f_v}, \quad (2.6)$$

where

$$Loss_u = \frac{1}{N_q} \sum_{i=1}^{N_q} |u(x_u^i, t_u^i) - u^i|^2, \quad (2.7)$$

$$Loss_v = \frac{1}{N_q} \sum_{i=1}^{N_q} |v(x_v^i, t_v^i) - v^i|^2, \quad (2.8)$$

$$Loss_{f_u} = \frac{1}{N_f} \sum_{j=1}^{N_f} |f_u(x_{f_u}^j, t_{f_u}^j)|^2, \quad (2.9)$$

$$Loss_{f_v} = \frac{1}{N_f} \sum_{j=1}^{N_f} |f_v(x_{f_v}^j, t_{f_v}^j)|^2, \quad (2.10)$$

here the initial and boundary value data about  $q(x, t)$  are denoted by  $\{x_u^i, t_u^i, u^i\}_{i=1}^{N_q}$  and  $\{x_v^i, t_v^i, v^i\}_{i=1}^{N_q}$ . Similarly, the collocations points for  $f_u(x, t)$  and  $f_v(x, t)$  are specified with  $\{x_{f_u}^j, t_{f_u}^j\}_{j=1}^{N_{f_u}}$  and  $\{x_{f_v}^j, t_{f_v}^j\}_{j=1}^{N_{f_v}}$ . The Loss function of Eq. (2.6) corresponds to the initial and boundary data and the structure imposed by Eq. (2.4) and (2.5) at a finite set

of collocation points. Specifically, the first and second terms on the right side of Eq. (2.6) attempt to fit the solution data, and the third and fourth terms learn to satisfy the  $f_u$  and  $f_v$ . The convergence of the loss function has been proved in Ref. [50]. In this paper, we simply choose to employ the L-BFGS algorithm to optimize all loss functions (2.6), which is a full-batch gradient-based optimization algorithm based on a quasi-Newton [51]. In addition, we use relatively simple multi-layer perceptrons with the Xavier initialization and the hyperbolic tangent (tanh) activation function [42]. All the code in this article is based on Python 3.0, and all numerical examples reported here are run on a DELL Precision 7920 Tower computer with 2.10 GHz 8-core Xeon Silver 4110 processor and 64 GB memory.

### 3. SOLITON SOLUTIONS AND BREATHER SOLUTION OF THE NONLINEAR SCHRÖDINGER EQUATION

The (1+1)-dimensional focusing nonlinear Schrödinger equation is a classical integrable field equation for describing quantum mechanical systems, nonlinear wave propagation in optical fibers or waveguides, Bose-Einstein condensates and plasma waves. In optics, the nonlinear term is generated by the intensity dependent index of a given material. Similarly, the nonlinear term for Bose-Einstein condensates is the result of the mean-field interactions about the interacting N-body system. We consider the focusing nonlinear Schrödinger equation along with Dirichlet boundary conditions given by

$$\begin{cases} iq_t + q_{xx} + 2|q|^2q = 0, x \in [x_0, x_1], t \in [t_0, t_1], \\ q(x, t_0) = q_0(x), \\ q(x_0, t) = q(x_1, t) = 0, \end{cases} \quad (3.1)$$

where  $x_0, x_1$  represent the lower and upper boundaries of  $x$  respectively. Similarly,  $t_0$  and  $t_1$  represent the initial and end times of  $t$  respectively.  $q_0(x)$  is an arbitrary complex-valued function. The first equation of Eq. (3.1) described the evolution of weakly nonlinear dispersive wave modulation. It arisen in the propagation of electromagnetic waves through matter. In view of the character of its solution, it was be calle “self focusing” nonlinear Schrödinger equation. For water wave modulation, there is usually coupling between modulation and wave induced current, so in some cases, water wave modulation can also be described by the nonlinear Schrödinger equation [2]. The N-soliton solutions and breather solution of the above equation have been obtained by many methods [36, 38, 52]. In this part, we will use the deep learning method to simulate the soliton solutions and breather solution, and compare it with the known exact solution, so as to prove that the numerical solution  $q(x, t)$  obtained by neural network is effective. From Ref. [52], we can derived the form of N-soliton solution of nonlinear Schrödinger equation, which is obtained by the Riemann Hilbert method. the N-soliton solution formulation shown as follow

$$q(x, t) = -2i \frac{\det R}{\det M}, \quad (3.2)$$

where  $M$  is a matrix of  $N \times N$ ,

$$M = \begin{bmatrix} M_{11} & M_{12} & \cdots & M_{1N} \\ M_{21} & M_{22} & \cdots & M_{2N} \\ \vdots & \vdots & \ddots & \vdots \\ M_{N1} & M_{N2} & \cdots & M_{NN} \end{bmatrix}, \quad (3.3)$$

and

$$M_{jk} = \frac{e^{-(\theta_k + \theta_j^*)} + c_j^* c_k e^{\theta_k + \theta_j^*}}{\zeta_j^* - \zeta_k}, \quad j, k = 1 \cdots N. \quad (3.4)$$

$R$  is a matrix of  $(N+1) \times (N+1)$  as

$$R = \begin{bmatrix} 0 & c_1 e^{\theta_1} & \cdots & c_N e^{\theta_N} \\ e^{-\theta_1^*} & M_{11} & \cdots & M_{1N} \\ \vdots & \vdots & \ddots & \vdots \\ e^{-\theta_N^*} & M_{N1} & \cdots & M_{NN} \end{bmatrix}, \quad (3.5)$$

where  $\theta_k = -i\zeta_k x - 2i\zeta_k^2 t$  ( $k = 1 \cdots N$ ),  $\zeta_k$  and  $c_i$  ( $i = 1 \cdots N$ ) are complex value constants. Therefore, after taking the value of positive integer  $N$ , one can obtain the corresponding N-soliton solution and breather solution of the nonlinear Schrödinger Eq. (2.1).

#### 3.1. One-soliton solution.

In this section, based on the neural network structure which contains nine hidden layers, each layer has 40 neurons, we numerically construct one-soliton solution of Eq. (3.1) via the deep learning method. When  $N = 1$ , we have

$R = \begin{pmatrix} 0 & c_1 e^{\theta_1} \\ e^{-\theta_1^*} & M_{11} \end{pmatrix}$ ,  $M_{11} = \frac{e^{-(\theta_1 + \theta_1^*)} + c_1^* c_1 e^{\theta_1 + \theta_1^*}}{\zeta_1^* - \zeta_1}$ ,  $\det R = -c_1 e^{\theta_1 - \theta_1^*}$ ,  $\det M = M_{11}$ , so the solution (3.2) is

$$q(x, t) = -2i \frac{\det R}{\det M} = 2i(\zeta_1^* - \zeta_1) \frac{c_1 e^{\theta_1 - \theta_1^*}}{e^{-(\theta_1 + \theta_1^*)} + |c_1|^2 e^{\theta_1 + \theta_1^*}}. \quad (3.6)$$

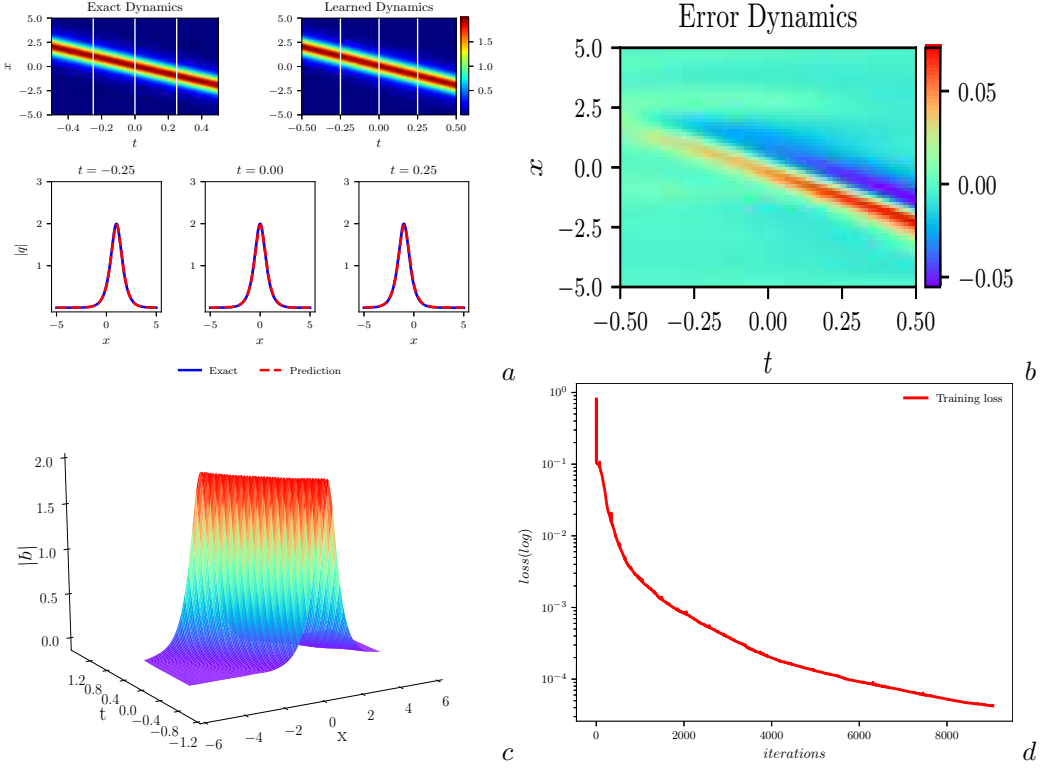


FIGURE 1. The one-soliton solution  $q(x, t)$ : (a) The density plots and the sectional drawing; (b) The error density plots; (c) The three-dimensional plots; (d) The iterative curve plots.

Letting

$$\zeta_1 = \xi + i\eta, \quad c_1 = e^{-2\eta x_0 + i\sigma_0},$$

where  $\xi, \eta$  are the real and imaginary parts of  $\zeta_1$ , and  $x_0, \sigma_0$  are real parameters, then the above one-soliton solution (3.6) can be reduced to

$$q(x, t) = 2\eta \operatorname{sech}[2\eta(x + 4\xi t - x_0)] e^{[-2i\xi x - 4i(\xi^2 - \eta^2)t + i\sigma_0]}. \quad (3.7)$$

One can obtain the exact one-soliton solution of the nonlinear Schrödinger Eq. (2.1) after taking  $\eta = 1, \xi = 1, x_0 = 0, \sigma_0 = 1$  into (3.7) as follow

$$q(x, t) = 2\operatorname{sech}(8t + 2x) e^{(-2ix + i)}. \quad (3.8)$$

Then we take  $[x_0, x_1]$  and  $[t_0, t_1]$  in Eq. (3.1) as  $[-5.0, 5.0]$  and  $[-0.5, 0.5]$ , respectively. The corresponding initial condition is obtained by substituting a specific initial value into (3.8)

$$q_0(x) = 2\operatorname{sech}(2x - 4) e^{(-2ix + i)}. \quad (3.9)$$

We employ the traditional finite differences on fixed grids method for simulating formula (3.9) to acquire original dataset with the help of MATLAB software. Specifically, we divide space  $[-5.0, 5.0]$  into 513 points and time  $[-0.5, 0.5]$  into 401 points, one-soliton solution  $q$  is discretized into  $[513 \times 401]$  snapshots accordingly. We generate a smaller training dataset that containing initial-boundary data by randomly extracting  $N_q = 100$  from original dataset and  $N_f = 10000$  collocation points which are generated by the Latin hypercube sampling method [53]. After giving a dataset of initial and boundary points, the latent one-soliton solution  $q(x, t)$  has been successfully learned by tuning all learnable parameters of the neural network and regulating the loss function (2.6). The model achieves a relative  $\mathbb{L}_2$  error of  $2.566069\text{e-}02$  in about 725.9232 seconds, and the number of iterations was 8324.

In Figure 1, the density plots, the sectional drawing of the latent one-soliton solution  $q(x, t)$ , the error diagram about the difference between exact one-soliton solution and hidden one-soliton solution, and the iteration number curve plots are plotted respectively. The (a) of Fig. 1 clearly compares the exact solution with the predicted spatiotemporal solution. Obviously, combining with the (b), we can see that the error between the numerical solution and the exact solution is very small. We particularly present a comparison between the exact solution and the predicted solution at different times  $t = -0.25, 0, 0.25$  in the bottom panel of (a). It is obvious that as time  $t$  increases, the one-soliton solution propagates along the negative direction of the  $x$ -axis. The 3D plots of the predicted solution and the algebraic curve satisfied by the number of iterations and loss function are given out in detail in (c) and (d) of Fig. 1. It is not difficult to see that the curve which revealing the relation between iteration number and loss function is very smooth and stable, and further verify the effectiveness and stability of the integrable deep learning method.

### 3.2. Two-soliton solution and breather solution.

In this section, based on the neural network architecture which contains nine hidden layers, each layer has 80 neurons, we numerically construct the two-soliton solution and breather solution of Eq. (3.1) by using the deep learning method. When  $N = 2$ , the solution (3.2) can also be written out explicitly. We have

$$F = \begin{pmatrix} 0 & c_1 e^{\theta_1} & c_2 e^{\theta_2} \\ e^{-\theta_1^*} & M_{11} & M_{12} \\ e^{-\theta_2^*} & M_{21} & M_{22} \end{pmatrix}, M = \begin{pmatrix} M_{11} & M_{12} \\ M_{21} & M_{22} \end{pmatrix},$$

and here

$$M_{11} = \frac{e^{-(\theta_1 + \theta_1^*)} + c_1^* c_1 e^{\theta_1 + \theta_1^*}}{\zeta_1^* - \zeta_1}, M_{12} = \frac{e^{-(\theta_2 + \theta_1^*)} + c_1^* c_2 e^{\theta_2 + \theta_1^*}}{\zeta_1^* - \zeta_2},$$

$$M_{21} = \frac{e^{-(\theta_1 + \theta_2^*)} + c_2^* c_1 e^{\theta_1 + \theta_2^*}}{\zeta_2^* - \zeta_1}, M_{22} = \frac{e^{-(\theta_2 + \theta_2^*)} + c_2^* c_2 e^{\theta_2 + \theta_2^*}}{\zeta_2^* - \zeta_2},$$

where  $\theta_1 = -i\zeta_1 x - 2i\zeta_1^2 t$ ,  $\theta_1^* = i\zeta_1^* x + 2i\zeta_1^{*2} t$ ,  $\theta_2 = -i\zeta_2 x - 2i\zeta_2^2 t$ ,  $\theta_2^* = -i\zeta_2^* x - 2i\zeta_2^{*2} t$ ,  $\zeta_j (j = 1, 2)$  are complex value constants, so one can derive the general form of two-soliton solution as follow

$$q(x, t) = 2i \frac{c_2 M_{11} e^{\theta_2 - \theta_2^*} - c_2 M_{12} e^{\theta_2 - \theta_1^*} - c_1 M_{21} e^{\theta_1 - \theta_2^*} + c_1 M_{22} e^{\theta_1 - \theta_1^*}}{M_{11} M_{22} - M_{12} M_{21}}. \quad (3.10)$$

According to the relationship between the two-soliton solution and the breather solution, we can know that when  $\text{Re}(\zeta_1) \neq \text{Re}(\zeta_2)$ , the solution  $q(x, t)$  is a two-soliton solution, and when  $\text{Re}(\zeta_1) = \text{Re}(\zeta_2)$ , the solution  $q(x, t)$  composes a bound state which also called the breather solution. We choose these appropriate parameters as

$$\zeta_1 = 0.1 + 0.7i, \quad \zeta_2 = -0.1 + 0.4i, \quad c_1 = c_2 = 1, \quad (3.11)$$

so we can obtain the exact two-soliton solution in the formulae (3.10) is

$$q(x, t) = \frac{-2iA}{B}, \quad (3.12)$$

where

$$A = (0.224 + 0.158i)e^{i(1.92t + 0.32it - 0.2x - 0.8ix)} - (0.224 + 0.232i)e^{-i(-0.6t + 0.56it - 0.2x + 1.4ix)} +$$

$$(0.224 - 0.232i)e^{i(0.6t + 0.56it + 0.2x + 1.4ix)} + (0.518i - 0.224)e^{-i(-1.92t + 0.32it + 0.2x - 0.8ix)},$$

$$B = 1.25e^{0.88t + 0.6x} + 0.13e^{-0.24t - 2.2x} + 1.25e^{-0.88t - 0.6x} - 1.12e^{i(1.32t - 0.4x)} - 1.12e^{-i(1.32t - 0.4x)} + 0.13e^{0.24t + 2.2x}.$$

On the other hand, if these parameters are selected as

$$\zeta_1 = 0.7i, \quad \zeta_2 = 0.4i, \quad c_1 = c_2 = 1, \quad (3.13)$$

one can obtain the exact breather solution

$$q(x, t) = \frac{-2i(-0.246ie^{-i(-0.64t + 1.4ix)} + 0.462ie^{-i(-1.96t - 0.8ix)} - 0.264ie^{i(0.64t + 1.4ix)} + 0.462ie^{-i(-1.96t + 0.8ix)})}{1.21e^{-0.6x} + 1.21e^{0.6x} - 1.12e^{1.32it} + 0.09e^{2.2x} - 1.12e^{-1.32it} + 0.09e^{-2.2x}}, \quad (3.14)$$

Now we take  $[x_0, x_1]$  and  $[t_0, t_1]$  in Eq. (3.1) as  $[-5.0, 5.0]$  and  $[-3.0, 3.0]$ , respectively. For instance, we consider the initial condition of two-soliton solution based on Eq. (3.12)

$$q_0(x) = \frac{-2iA'}{B'}, \quad (3.15)$$

where

$$A' = (0.224 + 0.158i)e^{i(-5.76 - 0.96i - 0.2x - 0.8ix)} - (0.224 + 0.232i)e^{-i(1.8 - 1.68i - 0.2x + 1.4ix)} +$$

$$(0.224 - 0.232i)e^{i(-1.8 - 1.68i + 0.2x + 1.4ix)} + (0.518i - 0.224)e^{-i(5.76 - 0.96i + 0.2x - 0.8ix)},$$

$$B' = 1.25e^{-2.64 + 0.6x} + 0.13e^{0.72 - 2.2x} + 1.25e^{2.64 - 0.6x} - 1.12e^{i(-3.96 - 0.4x)} - 1.12e^{-i(-3.96 - 0.4x)} + 0.13e^{-0.72 + 2.2x}.$$

Similarly, the initial condition of breather solution is as follows

$$q_0(x) = \frac{-2i(-0.246ie^{-i(1.92 + 1.4ix)} + 0.462ie^{-i(5.88 - 0.8ix)} - 0.264ie^{i(-1.92 + 1.4ix)} + 0.462ie^{-i(5.88 + 0.8ix)})}{1.21e^{-0.6x} + 1.21e^{0.6x} - 1.12e^{-3.96i} + 0.09e^{2.2x} - 1.12e^{3.96i} + 0.09e^{-2.2x}}. \quad (3.16)$$

Then adopting the same data generation and sampling method in Section 2.1, and we numerically simulate the two-soliton solution and the breather solution of the nonlinear Schrödinger equation (2.1) by the deep learn method. In training the two-soliton solution, the neural network achieves a relative  $\mathbb{L}_2$  error of  $5.500792e-02$  in about 2565.0818 seconds, and the number of iterations was 17789. However, the network model for learning breather solution achieves a relative  $\mathbb{L}_2$  error of  $9.689267e-03$  in about 1934.2586 seconds, and the number of iterations was 13488. Apparently, since the breathing solution is a special form of the two-soliton solution, the training of the breather solution takes less time, the number of iterations is less, the relative error is smaller, and the overall effect is better than training of the two-soliton solution.

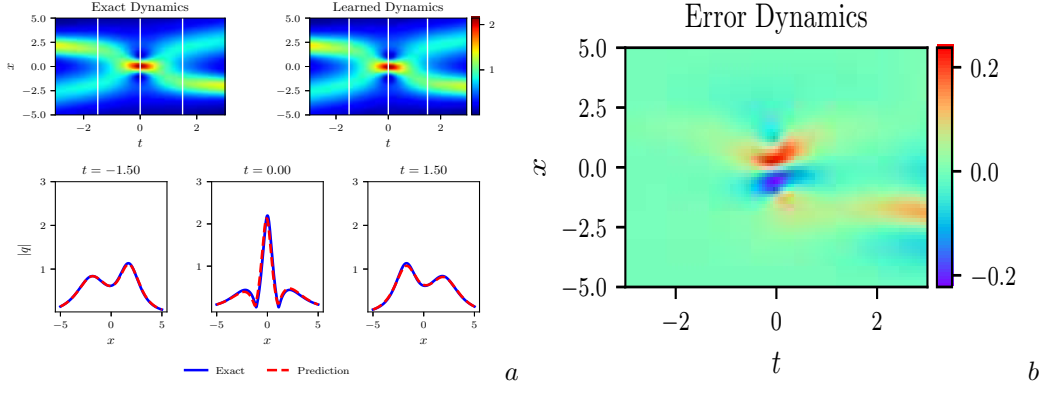


FIGURE 2. The two-soliton solution  $q(x, t)$ : (a) The density plots and the sectional drawing; (b) The error density plots.

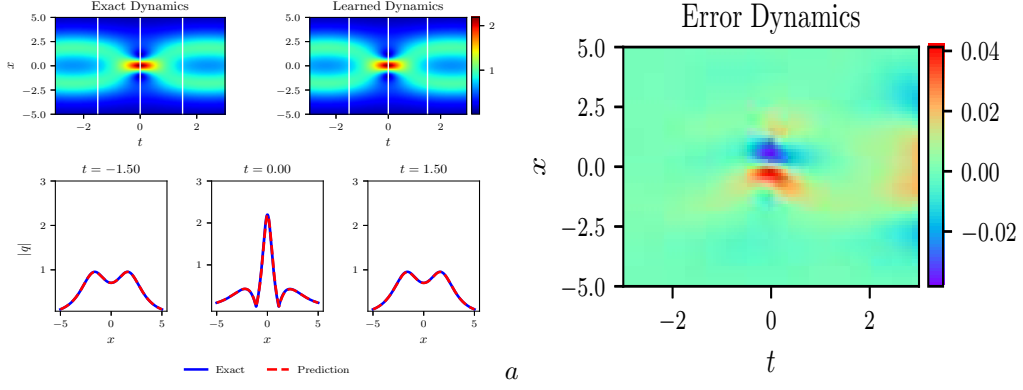


FIGURE 3. The breather solution  $q(x, t)$ : (a) The density plots and the sectional drawing; (b) The error density plots.

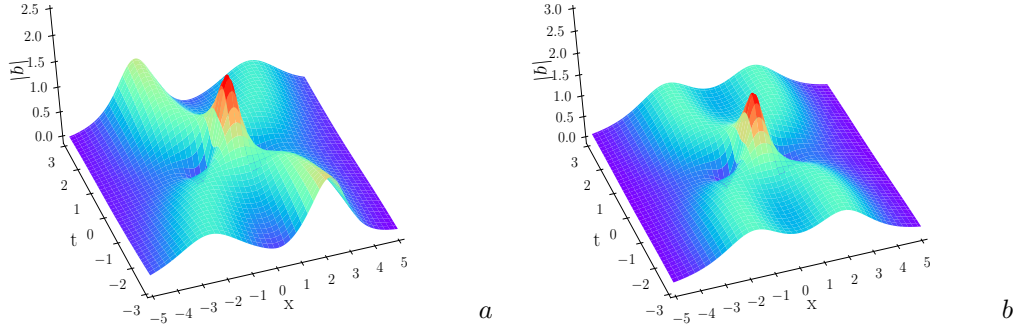


FIGURE 4. The plot3d of  $q(x, t)$ : (a) The plot3d of the two-soliton solution; (b) The plot3d of the breather solution.

Fig. 2 and Fig. 3 show the density plots, profile and error density plots of the two-soliton solution and the breather solutions, respectively. From the bottom panel of (a) in Fig. 2, we can clearly see that the intersection of two solitary waves with different wave widths and amplitudes produces a peak of higher amplitude, which satisfies the law of conservation of energy. At  $t = -1.50, 0, 1.50$ , we reveal the profiles of the three moments respectively, and find that the amplitude is the largest when  $t = 0$ . According to the relevant knowledge of soliton theory, we know that two solitary waves have elastic collision. Similarly, one can look at the breather solution which has been shown in (a) of Fig. 3 is a special bound state two-soliton solution formed by two solitary waves with the same wave velocity, wave width and amplitude, and has periodicity with time  $t$ . The (b) of Fig. 2 and Fig. 3 show the error dynamics of the difference between the exact solution and the predicted solution for the two-soliton solution and the breather solution. In Fig. 4, the corresponding plot3d of the two-soliton solution and the breather solution are plotted respectively. It is evident that the breather solution is more symmetric than the general 2-soliton solution.

For the numerical simulation of the three-soliton solution, we only need to take  $N = 3$  in Eqs. (3.2)-(3.5) to get the exact solution of the three-soliton solution, and discretize the initial and boundary value data of the exact solution

as our original data set and substitute it into our deep learning algorithm to simulate the corresponding three-soliton solution numerically. Similarly, N-soliton solutions can be learned by the same method. Of course, the higher the order of soliton solution, the more complex the form of the solution, the higher the computational load of the neural network and the longer the training time.

#### 4. ROGUE WAVE SOLUTIONS OF THE NONLINEAR SCHRÖDINGER EQUATION

Recently, the research of rogue wave is one of the hot topics, which encompassing many aspects such as optics, ocean dynamics, plasma, Bose-Einstein condensate and even finance [8,9,54–56]. In addition to the peak amplitude more than twice of the background wave, rogue waves also have the characteristics of instability and unpredictability. Therefore, the study and application of rogue waves play an momentous role in real life, especially how to avoid the damage to ships caused by ocean rogue waves is of great practical significance. As a one-dimensional integrable scalar equation, nonlinear Schrödinger equation plays a key role in describing rogue waves. In 1983, Peregrine first gave a rational rogue waves to the NLS equation, whose generation principle is identified as the evolution of the breather waves when the period tends to infinity [2]. At present, the researches on rogue wave of nonlinear Schrödinger equation through machine learning are relatively less. Marcucci et al. have studied the computational machine in which nonlinear waves replace the internal layers of neural networks, discussed learning conditions, and demonstrated functional interpolation, data interpolation, data sets, and Boolean operations. When the nonlinear Schrödinger equation is considered, the use of highly nonlinear regions means that solitons, rogue waves and shock waves play a leading role in the training and calculation [16]. In wave solutions of the nonlinear Schrödinger equation (2.1) by the deep learn method. Here, we consider the another form of focusing nonlinear Schrödinger equation along with Dirichlet boundary conditions given by

$$\begin{cases} iq_t + \frac{1}{2}q_{xx} + |q|^2q = 0, x \in [x_0, x_1], t \in [t_0, t_1], \\ q(x, t_0) = q_0(x), \\ q(x_0, t) = q(x_1, t) = 1, \end{cases} \quad (4.1)$$

where  $x_0, x_1$  represent the lower and upper boundaries of  $x$  respectively. Similarly,  $t_0$  and  $t_1$  represent the initial and end times of  $t$  respectively.  $q_0(x)$  is an arbitrary complex-valued function. The boundary condition of Eq. (4.1) is different from equation (3.1) because the rogue wave tends to 1 when  $t$  tends to infinity. The rogue wave solutions of Eq. (4.1) have been obtained by many ways. Therefore, we can gain respectively the one-order rogue wave and the two-order rogue wave of Eq. (4.1) from Ref. [11] as follow

$$q(x, t) = \left(1 - \frac{4(1 + 2it)}{4t^2 + 4x^2 + 1}\right) e^{it}, \quad (4.2)$$

and

$$q(x, t) = \left(1 + \frac{G + itH}{D}\right) e^{it}, \quad (4.3)$$

where

$$\begin{aligned} G &= \frac{3}{8} - 3x^2 - 2x^4 - 9t^2 - 10t^4 - 12t^2x^2, \\ H &= \frac{15}{4} + 6x^2 - 4x^4 - 2t^2 - 4t^4 - 8t^2x^2, \\ D &= \frac{3}{32} + \frac{9}{8}x^2 + \frac{1}{2}x^4 + \frac{2}{3}x^6 + \frac{33}{8}t^2 + \frac{9}{2}t^4 + \frac{2}{3}t^6 - 3t^2x^2 + 2t^2x^4 + 2t^4x^2. \end{aligned}$$

In the latter two parts, we will construct the initial and boundary value dataset to train our prediction solutions based on the above two rogue wave solutions by constructing a neural network with nine hidden layers, each layer has 40 neurons.

##### 4.1. One-order rogue wave.

In this section, we will numerically learning the one-order rogue wave of the nonlinear Schrödinger equation by constructing the neural network. Then we take  $[x_0, x_1]$  and  $[t_0, t_1]$  in Eq. (4.1) as  $[-2.0, 2.0]$  and  $[-1.5, 1.5]$ , respectively. The corresponding initial condition is obtained by substituting a specific initial value into (4.2), we have

$$q_0(x) = \left(1 + \frac{-4 + 12i}{4x^2 + 10}\right) e^{-1.5i}. \quad (4.4)$$

Next, we obtain the initial and boundary value data set by the same data discretization method in Section 2.1, and then we can simulate precisely one-order rogue wave solution by substituting dataset into the deep learning algorithm which is composed of neural network model. By randomly selecting  $N_q = 100$  from the original dataset and  $N_f = 10000$  configuration points which are generated by Latin hypercube sampling method, a complete training data set containing initial boundary data is generated. The neural network model achieves a relative  $\mathbb{L}_2$  error of  $7.845201e-03$  in about 870.6575 seconds, and the number of iterations was 9584.

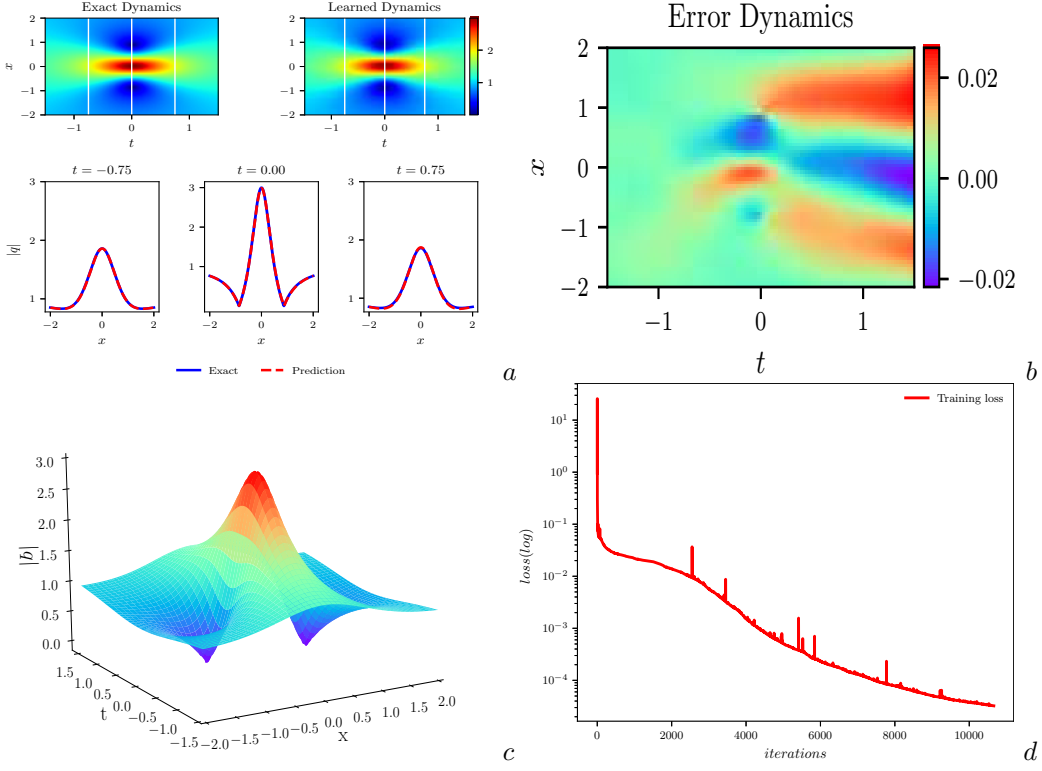


FIGURE 5. The one-order rogue wave solution  $q(x, t)$ : (a) The density plots and the sectional drawing; (b) The error density plots; (c) The three-dimensional plots; (d) The iterative curve plots.

The results of our experiment have been summarized in Fig. 5, and we simulate the solution of  $q(x, t)$  and obtain the density plots, profile, error dynamics plots, 3Dplots and iteration number curve plots of the one-order rogue wave. Specifically, the magnitude of the predicted spatio-temporal solution  $|q(x, t)|$  has shown in the top panel of Figure (a). It can be simply seen that the amplitude of the rogue wave solution changes greatly in a short time from the bottom panel of Figure (a) in Fig. (5). Furthermore, we present a comparison between the exact and the predicted solution at different time instants  $t = -0.75, 0, 0.75$ . Figure (b) reveal the relative  $\mathbb{L}_2$  error after time  $t > 0$  is greater than that of time  $t < 0$ . From figure d of Fig. 5, we can realise that when the number of iterations is more than 2000, there will be some obvious fluctuations which we could call "burr" in the training loss function, it does not exist in the iterative process about the one-soliton solution of the nonlinear Schrödinger equation. Utilizing only a handful of initial data, one can accurately capture the intricate nonlinear dynamic behavior of the Schrödinger equation by the deep learning method.

In addition, based on the same initial and boundary values of the one-order rogue waves in the case of  $N_q = 100$  and  $N_f = 10000$ , we employ the control variable method which is often used in physic to study the effects of different levels of neural networks and different numbers of single-layer neurons on the one-order rogue wave dynamics of nonlinear Schrödinger equation. Moreover, the relative  $\mathbb{L}_2$  errors of different layers of neural networks and different numbers of single-layer neurons are given in Table 1. From the data in Table 1, we can see that when the number of neural network layers is fixed, the more the number of single-layer neurons, the smaller the relative error. Of course, due to the influence of randomness, there are individual data results that do not meet the previous conclusion, but on the whole the conclusion is tenable. However, when the number of single-layer neurons is fixed, the influence of the number of neural network layers on the relative error is not obvious. To sum up, we can draw the conclusion that the number of layers of neural network and the number of single-layer neurons jointly determine the relative  $\mathbb{L}_2$  error, but the number of monolayer neurons has a relatively large impact. In the case of the same original dataset, table 2 shows the relative  $\mathbb{L}_2$  error of 9-layer neural network and single-layer neural network with 40 neurons when taking different number of sampling points  $N_q$  in the initial-boundary data and different number of collocation points  $N_f$  which are generated by the Latin hypercube sampling method. From the table 2, we can see that the influences of  $N_q$  and  $N_f$  on the relative  $\mathbb{L}_2$  error of neural network are not so obvious, which also explain why the neural network model can simulate more accurate numerical solutions with smaller data set.

#### 4.2. Two-order rogue wave.

In the next example, we consider the two-order rogue wave of the nonlinear Schrödinger equation, and properly take  $[x_0, x_1]$  and  $[t_0, t_1]$  in Eq. (4.1) as  $[-2.0, 2.0]$  and  $[-0.5, 0.5]$ . Here we consider the corresponding initial condition

TABLE 1. One-order rogue wave of the nonlinear Schrödinger equation: Relative final prediction error measure in the  $\mathbb{L}_2$  norm for different number of hidden layers and neurons in each layer.

Neurons Layers	20	30	40	50	60
5	2.765905e-03	2.903368e-04	4.961406e-04	5.232502e-04	9.323978e-04
7	2.699082e-03	1.328768e-03	4.030658e-04	3.633812e-04	1.448091e-03
9	2.732954e-03	2.618465e-03	7.845201e-03	6.880915e-04	6.797486e-04
11	4.641999e-03	1.779715e-03	1.440061e-03	9.148106e-04	1.581767e-03

TABLE 2. One-order rogue wave of the nonlinear Schrödinger equation: Relative final prediction error measure in the  $\mathbb{L}_2$  norm for different number of  $N_q$  and  $N_f$ .

$N_f$ $N_q$	6000	8000	10000	12000	14000
80	1.473695e-02	9.200569e-03	7.967294e-03	6.034213e-03	3.575678e-03
100	1.176106e-02	3.082057e-03	7.845201e-03	5.495886e-03	1.332274e-02
120	1.525780e-02	1.265775e-02	4.175621e-02	2.402183e-03	6.568740e-03

which has been obtained by substituting a specific initial time into (4.3) as follows

$$q_0(x) = \left(1 + \frac{-70.5 - 30x^2 - 2x^4 - 1.5i(-21 - 12x^2 - 4x^4)}{39.75 + 4.5x^2 + 5x^4 + \frac{2}{3}x^6}\right) e^{-1.5i}. \quad (4.5)$$

We use the same data discretization method in Section 2.1 for getting the initial and boundary value data sets. In the neural network algorithm which have received the initial and boundary value data set, initial and boundary value data of  $N_q = 100$  are randomly selected from the initial and boundary value data. In addition, configuration points of  $N_f = 10000$  are extracted by Latin hypercube sampling method. Finally, the hidden two-order rogue wave solution of nonlinear Schrödinger equation is approximated infinitely by constraining loss function. The neural network model achieves a relative  $\mathbb{L}_2$  error of 1.665401e-02 in about 1090.0317 seconds, and the number of iterations was 11450.

The detailed illustration is given out, as shown in Fig. 6. The top panel of figure (a) of Fig. 6 gives the density map of hidden solution  $q(x, t)$ , and when combining with the bottom panel of figure (a) and figure (b), we can see that the relative error is relatively large at  $t = 0.25$ . As for figure (d), the fluctuation(burr phenomenon) of loss function is obvious when the number of iterations is less than 3000, which is just the opposite of the first order strange wave solution.

## 5. CONCLUSION

In this paper, we introduce deep learning method based on physical-informed neural network, which is a new numerical method to solve integrable equations by universal function approximators. It can code and simulate many kinds of solutions of integrable equations with a given data set. This method showcases a series of known results of various problems in the interdisciplinary field of applied mathematics and computational science, and opens a path for using deep learning to simulate unknown solutions and unknown equations of integrable equations which containing powerful mathematical and physical ability. We apply the data-driven algorithm to deduce the soliton solutions, the breather solution and the rogue wave solutions of the nonlinear Schrödinger equation by establishing deep learning neural network framework with high computational efficiency. We outline how different types of solutions (such as general soliton solutions, breather solution and rogue wave solutions) are generated due to different choices of initial and boundary value data. Remarkably, these results show that the deep learning method can recover the different dynamic behaviors of integrable equation well. Furthermore, the sizes of space-time variable  $x$  and  $t$  interval are selected by whether the dynamic behavior of these solutions can be well simulated after a lot of experiments in this paper. However, for the breathers, the wider the interval of time variable  $t$ , the better the dynamic behavior can be seen. We have tried a wider range of time interval  $t$ , but the training effect is not very good. So more complex boundary conditions, such as Neumann boundary conditions, may be considered. Similarly, for the integrable complex mKdV equation, the Dirichlet boundary conditions can not simulate the ideal rogue wave solutions. In addition, the influence of noise on our neural network model is not introduced in this paper. However, this kind of objective physical factors in real life need to be considered in the future research. more general nonlinear Schrodinger equation, such as the derivative Schrodinger equation, will be investigated more in the next work. These new problems need more research and training in future.

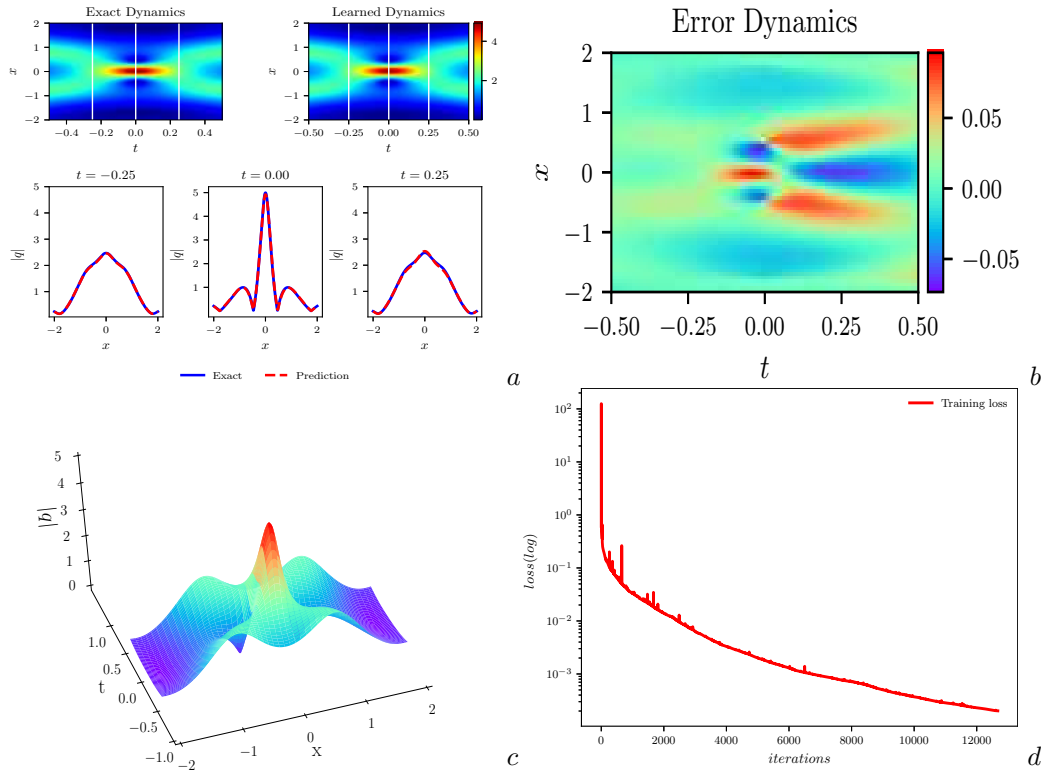


FIGURE 6. The two-order rogue wave solution  $q(x, t)$ : (a) The density plots and the sectional drawing; (b) The error density plots; (c) The three-dimensional plots; (d) The iterative curve plots.

## REFERENCES

- [1] Draper L 1965 ‘Freak’ ocean, Mar. Obs. 35 193-195
- [2] Peregrine D H 1983 Water waves, nonlinear Schrödinger equations and their solutions, J. Aust. Math. Soc. Ser. B 25 16-43
- [3] Zakusky N J and Kruskal M D 1965 Interaction of solitons in a collisionless plasma and the recurrence of initial states, Phys. Rev. Lett. 15 24 0-243
- [4] Parkins A and Walls D 1998 The physics of trapped dilute-gas Bose-Einstein condensates, Phys. Rep. 303(1) 1-80
- [5] Ablowitz M J and Clarkson P 1992 Solitons, Nonlinear Evolution Equations and Inverse Scattering (Cambridge University Press, Cambridge, UK)
- [6] Schrödinger E 1926 An undulatory theory of the mechanics of atoms and molecules, Phys. Rev. 25 1049-1070
- [7] Guo B L, Ling L M and Liu Q P 2012 High-order solution and generalized Darboux transformation of derivative nonlinear Schrödinger equation, Schrödinger equation, Stud. Appl. Math. 130, 317-344
- [8] Solli D R, Ropers C, Koonath P and Jalali B 2007 Optical rogue waves, Nature 450 1054-1057
- [9] Chabchoub A, Hoffmann N P and Akhmediev N 2011 Rogue wave observation in a water wave tank, Phys. Rev. Lett. 106 204502
- [10] Qiao Z J 1994 A hierarchy of nonlinear evolution equations and finite-dimensional involutive systems, J. Math. Phys. 35(6) 2971-2977
- [11] Akhmediev N, Ankiewicz A and Soto-Crespo J M 2009 Rogue waves and rational solutions of the nonlinear Schrödinger equation, Phys. Rev. E 80 026601
- [12] Ohta Y and Yang J K 2012 General high-order rogue wave and their dynamics in the nonlinear Schrödinger equation, Proc. R. Soc. Lond. Sect. A 468 1716-1740
- [13] Hasegawa A and Tappert F 1973 Transmission of stationary nonlinear optical pulses in dispersive dielectric fibers. I. Anomalous dispersion, Appl. Phys. Lett. 23 142-144
- [14] Kavitha L and Daniel M 2003 Integrability and soliton in a classical one-dimensional site-dependent biquadratic Heisenberg spin chain and the effect of nonlinear inhomogeneity, J. Phys. A 36(42) 10471-10492
- [15] Qiao Z J 1993 A new completely integrable Liouville’s system produced by the Kaup-Newell eigenvalue problem, J. Math. Phys. 34(7) 3110-3120
- [16] Marcucci G, Pierangeli D, and Conti C 2020 Theory of neuromorphic computing by waves: machine learning by rogue waves, dispersive shocks, and solitons, Phys. Rev. Lett. 125 093901
- [17] Mitchell T M 1997 Machine Learning (McGraw-Hill series in computer science)
- [18] Bishop C M 2006 Pattern Recognition and Machine Learning (Springer)
- [19] Alipanahi B, Delong A, Weirauch M T and Frey B J 2015 Predicting the sequence specificities of DNA- and RNA-binding proteins by deep learning, Nat. Biotechnol. 33 831-838
- [20] Duda R O, Hart P E and Stork D G 2000 Pattern Classification (Wiley-Interscience)
- [21] Lake B M, Salakhutdinov R and Tenenbaum J B 2015 Human-level concept learning through probabilistic program induction, Science 350(6266) 1332-1338
- [22] Krizhevsky A, Sutskever I and Hinton G E 2012 ImageNet classification with deep convolutional neural networks, Proceedings of the 25th International Conference on Neural Information Processing Systems, Lake Tahoe, 3-6 December 2012, 1097-1105.
- [23] McCulloch W S and Pitts W 1943 A logical calculus of the ideas immanent in nervous activity, Bull. Math. Biophys. 5 115-133
- [24] Rosenblatt F 1958 The perceptron: a probabilistic model for information storage and organization in the brain, Psychological Review 65(6) 386-408

- [25] Bryson A E and Ho Y C 1969 Applied Optimal Control: Optimization, Estimation, and Control (Blaisdell Publishing Company or Xerox College Publishing)
- [26] Krizhevsky A, Sutskever I and Hinton G E 2017 ImageNet classification with deep convolutional neural networks, Communications of the Acm 60(6) 84-90
- [27] Hornik K, Stinchcombe M and White H 1989 Multilayer feedforward networks are universal approximators, Neural Netw. 2 359-366
- [28] Lagaris I E, Likas A and Fotiadis D I 1998 Artificial neural networks for solving ordinary and partial differential equations, IEEE Transactions on Neural Networks 9(5) 987-1000
- [29] LeCun Y, Bengio Y and Hinton G 2015 Deep learning, Nature 521 436-444
- [30] Raissi M, Perdikaris P and Karniadakis G E 2019 Physics-informed neural networks: A deep learning framework for solving forward and inverse problems involving nonlinear partial differential equations, J. Comput. Phys. 378 686-707
- [31] Jagtap A D, Kharazmi E and Karniadakis G E 2020 Conservative physics-informed neural networks on discrete domains for conservation laws: Applications to forward and inverse problems, Comput. Methods Appl. Mech. Engrg. 365 113028
- [32] Lax P D 1968 Integrals of nonlinear equations of evolution and solitary waves, Comm. Pure. Appl. Math. 21 467-490
- [33] Yu S J, Toda K and Fukuyama T 1998 N-soliton solutions to a (2+1)-dimensional integrable equation, J. Phys. A Math. Gen. 31 10181-10186
- [34] Iwao M and Hirota R 1997 Soliton solutions of a coupled modified KdV equations, J. Phys. Soc. Japan. 66(3) 577-588
- [35] Osman M S, Ghanbari B and Machado J A T 2019 New complex waves in nonlinear optics based on the complex Ginzburg-Landau equation with Kerr law nonlinearity, Eur. Phys. J. Plus 134 20
- [36] Hirota R 2004 Direct Methods in Soliton Theory (Springer-verlag, Berlin)
- [37] Geng X G and Tam H W 1999 Darboux transformation and soliton solutions for generalized nonlinear Schrödinger equations, J. Phys. Soc. Jpn. 68 1508-1512
- [38] Matveev V B and Salle M A 1991 Darboux Transformation and Solitons (Springer, Berlin, 1991)
- [39] Olver P J 1993 Applications of Lie Groups to Differential Equations (Springer, New York, 1993)
- [40] Zakharov V E, Manakov S V, Novikov S P and Pitaevskii L P 1984 The Theory of Solitons: The Inverse Scattering Method (Consultants Bureau, New York)
- [41] Pu J C and Chen Y 2020 Nonlocal Symmetries, Bäcklund Transformation and Interaction Solutions for the Integrable Boussinesq Equation, Modern Phys. Lett. B in press
- [42] Li J and Chen Y 2020 Solving second-order nonlinear evolution partial differential equations using deep learning, Commun. Theor. Phys. 72 105005
- [43] Bongard J and Lipson H 2007 Automated reverse engineering of nonlinear dynamical systems, Proc. Natl. Acad. Sci. USA. 104 9943-9948
- [44] Raissi M, Perdikaris P and Karniadakis G E 2017 Machine learning of linear differential equations using Gaussian processes, J. Comput. Phys. 348 683-693
- [45] Li J and and Chen Y 2020 A deep learning method for solving third-order nonlinear evolution equations, Commun. Theor. Phys. 72 115003
- [46] Li J and and Chen Y 2020 A physics-constrained deep residual network for solving the sine-Gordon equation, Commun. Theor. Phys. in press
- [47] Lou S Y 1997 An (n+1)-dimensional integrable model: Painlevé test, Commun. Theor. Phys. 28(2) 129-132
- [48] Tu G Z 1989 On Liouville integrability of zero-curvature equations and the yang hierarchy, J. Phys. A: Math. Gen. 22 2375-2392
- [49] Baydin A G, Pearlmutter B A, Radul A A and Siskind J M 2018 Automatic Differentiation in Machine Learning: a Survey, J. Mach. Learning Research 18(153) 1-43
- [50] Choromanska A, Henaff M, Mathieu M, Arous G B and Lecun Y 2015 Proceedings of the 18th International Conference on Artificial Intelligence and Statistics (AISTATS) 38
- [51] Liu D C and Nocedal J 1989 On the limited memory BFGS method for large scale optimization, Math. Program. 45 503-528
- [52] Yang J K 2010 Nonlinear Waves in Integrable and Nonintegrable Systems (SIAM, Philadelphia)
- [53] Stein M L 1987 Large sample properties of simulations using latin hypercube sampling, Technometrics 29(2) 143-151.
- [54] Bludov Y V, Konotop V V and Akhmediev N 2009 Matter rogue waves, Phys. Rev. A 80 033610
- [55] Moslem W M 2011 Langmuir rogue wave in electron-positron plasmas, Phys. Plasmas 18 032301
- [56] Yan Z Y 2011 Financial Rogue waves appearing in the coupled nonlinear volatility and option pricing model, Phys. Lett. A 375, 4274

(JP) SCHOOL OF MATHEMATICAL SCIENCES, SHANGHAI KEY LABORATORY OF PURE MATHEMATICS AND MATHEMATICAL PRACTICE, AND SHANGHAI KEY LABORATORY OF TRUSTWORTHY COMPUTING, EAST CHINA NORMAL UNIVERSITY, SHANGHAI 200241, PEOPLE'S REPUBLIC OF CHINA

(JL) SHANGHAI KEY LABORATORY OF TRUSTWORTHY COMPUTING, EAST CHINA NORMAL UNIVERSITY, SHANGHAI 200062, PEOPLE'S REPUBLIC OF CHINA

(YC) SCHOOL OF MATHEMATICAL SCIENCES, SHANGHAI KEY LABORATORY OF PURE MATHEMATICS AND MATHEMATICAL PRACTICE, AND SHANGHAI KEY LABORATORY OF TRUSTWORTHY COMPUTING, EAST CHINA NORMAL UNIVERSITY, SHANGHAI 200241, PEOPLE'S REPUBLIC OF CHINA

(YC) COLLEGE OF MATHEMATICS AND SYSTEMS SCIENCE, SHANDONG UNIVERSITY OF SCIENCE AND TECHNOLOGY, QINGDAO 266590, PEOPLE'S REPUBLIC OF CHINA

(YC) DEPARTMENT OF PHYSICS, ZHEJIANG NORMAL UNIVERSITY, JINHUA 321004, PEOPLE'S REPUBLIC OF CHINA  
*Email address: ychen@sei.ecnu.edu.cn*